

AFRL-VA-WP-TR-2006-3211

**LOW-SPEED FLOW CONTROL USING
DIELECTRIC BARRIER DISCHARGE
(DBD)**



Jordi Estevadeordal and Sivaram Gogineni

Aerodynamic Configuration Branch (AFRL/VAAA)
Aeronautical Sciences Division
Air Vehicles Directorate
Air Force Materiel Command, Air Force Research Laboratory
Wright-Patterson Air Force Base, OH 45433-7542

DECEMBER 2006

Final Report for 01 May 2005 – 01 December 2006

Approved for public release; distribution is unlimited.

STINFO COPY

**AIR VEHICLES DIRECTORATE
AIR FORCE MATERIEL COMMAND
AIR FORCE RESEARCH LABORATORY
WRIGHT-PATTERSON AIR FORCE BASE, OH 45433-7542**

NOTICE AND SIGNATURE PAGE

Using Government drawings, specifications, or other data included in this document for any purpose other than Government procurement does not in any way obligate the U.S. Government. The fact that the Government formulated or supplied the drawings, specifications, or other data does not license the holder or any other person or corporation; or convey any rights or permission to manufacture, use, or sell any patented invention that may relate to them.

This report was cleared for public release by the Air Force Research Laboratory Wright Site (AFRL/WS) Public Affairs Office and is available to the general public, including foreign nationals.

Copies may be obtained from the Defense Technical Information Center (DTIC) (<http://www.dtic.mil>).

AFRL-VA-WP-TR-2006-3211 HAS BEEN REVIEWED AND IS APPROVED FOR PUBLICATION IN ACCORDANCE WITH ASSIGNED DISTRIBUTION STATEMENT.

*/Signature//

ROGER L. KIMMEL
Project Engineer
Analytical Structural Mechanics Branch

//Signature//

CARL P. TILMANN
Technical Advisor
Analytical Structural Mechanics Branch

//Signature//

MICHAEL J. STANEK, Ph.D.
Technical Advisor
Aeronautical Sciences Division

This report is published in the interest of scientific and technical information exchange, and its publication does not constitute the Government's approval or disapproval of its ideas or findings.

*Disseminated copies will show “//signature//” stamped or typed above the signature blocks.

REPORT DOCUMENTATION PAGE

*Form Approved
OMB No. 0704-0188*

The public reporting burden for this collection of information is estimated to average 1 hour per response, including the time for reviewing instructions, searching existing data sources, searching existing data sources, gathering and maintaining the data needed, and completing and reviewing the collection of information. Send comments regarding this burden estimate or any other aspect of this collection of information, including suggestions for reducing this burden, to Department of Defense, Washington Headquarters Services, Directorate for Information Operations and Reports (0704-0188), 1215 Jefferson Davis Highway, Suite 1204, Arlington, VA 22202-4302. Respondents should be aware that notwithstanding any other provision of law, no person shall be subject to any penalty for failing to comply with a collection of information if it does not display a currently valid OMB control number. **PLEASE DO NOT RETURN YOUR FORM TO THE ABOVE ADDRESS.**

1. REPORT DATE (DD-MM-YY) December 2006			2. REPORT TYPE Final			3. DATES COVERED (From - To) 05/01/2005 – 12/01/2006		
4. TITLE AND SUBTITLE LOW-SPEED FLOW CONTROL USING DIELECTRIC BARRIER DISCHARGE (DBD)			5a. CONTRACT NUMBER In-house					
			5b. GRANT NUMBER					
			5c. PROGRAM ELEMENT NUMBER 62201F					
6. AUTHOR(S) Jordi Estevadeordal and Sivaram Gogineni			5d. PROJECT NUMBER A04R					
			5e. TASK NUMBER					
			5f. WORK UNIT NUMBER OB					
7. PERFORMING ORGANIZATION NAME(S) AND ADDRESS(ES) Aerodynamic Configuration Branch (AFRL/VAAA) Aeronautical Sciences Division Air Vehicles Directorate Air Force Materiel Command, Air Force Research Laboratory Wright-Patterson Air Force Base, OH 45433-7542			8. PERFORMING ORGANIZATION REPORT NUMBER AFRL-VA-WP-TR-2006-3211					
			9. SPONSORING/MONITORING AGENCY NAME(S) AND ADDRESS(ES) Air Vehicles Directorate Air Force Research Laboratory Air Force Materiel Command Wright-Patterson Air Force Base, OH 45433-7542					
10. SPONSORING/MONITORING AGENCY ACRONYM(S) AFRL-VA-WP			11. SPONSORING/MONITORING AGENCY REPORT NUMBER(S) AFRL-VA-WP-TR-2006-3211					
			12. DISTRIBUTION/AVAILABILITY STATEMENT Approved for public release; distribution is unlimited.					
13. SUPPLEMENTARY NOTES Report contains color. PAO Case Number: AFRL/WS 06-2809, 06 Dec 2006.			14. ABSTRACT DBDs were created in a quiescent environment, and particle image velocimetry (PIV) was used to obtain field measurements of velocity induced by the discharge. These PIV measurements included random phase measurements and measurements phase-locked to the DBD driving frequency. Instantaneous and average velocity distributions were used for flow analysis. In addition, the effects of buoyancy and large-scale background air movement around the test device were also evaluated and efforts to eliminate or minimize spurious results arising from either effect were made.					
			15. SUBJECT TERMS Plasma, Flow Control, Dielectric barrier discharge					
16. SECURITY CLASSIFICATION OF:			17. LIMITATION OF ABSTRACT: SAR		18. NUMBER OF PAGES 24		19a. NAME OF RESPONSIBLE PERSON (Monitor) Roger L. Kimmel	
a. REPORT Unclassified			b. ABSTRACT Unclassified		c. THIS PAGE Unclassified		19b. TELEPHONE NUMBER (Include Area Code) N/A	

Standard Form 298 (Rev. 8-98)
Prescribed by ANSI Std. Z39-18

1. Introduction

The use of dielectric barrier discharges (DBD) for subsonic flow control has received increasing attention over the past several years. Despite numerous applications for DBD's, the fundamental mechanism of their operation is still unknown. For this reason, a detailed examination of the plasma flow actuation mechanism was conducted and the following experiments were performed.

DBD discharges were created in a quiescent environment and particle image velocimetry (PIV) was used to obtain field measurements of velocity induced by the discharge. These PIV measurements included random phase measurements and measurements phase-locked to the DBD driving frequency. Instantaneous and average velocity distributions were used for flow analysis.

In addition the effects of buoyancy and large-scale background air movement around the test device were also evaluated and efforts to eliminate or minimize spurious results arising from either effect were made.

2. Experimental Set-up

2.1 Facility Description

An experimental facility was designed in order to create a quiescent environment for the flow generated by the DBD and is shown in Fig. 1. This figure shows the dimensions of the enclosure box made of Plexiglas for optical access that housed the DBD. The DBD configuration is shown in its side and top views in Figures 2 and 3. The DBD consists of two parallel copper electrodes (6.35 mm width) separated by dielectric barrier made of Kapton. In this configuration one electrode is covered and the other one uncovered. The spanwise length of the DBD was 63.5 mm. High-frequency, high-voltage is applied between the two electrodes to generate the plasma which generated a wall jet. The electrodes strip connections were positioned toward downstream of the wall jet flow to minimize upstream perturbations (Fig. 4). Honeycomb was installed on two sides to minimize ambient perturbations, closed-box recirculations, and to facilitate PIV seeding. The DBD was installed in one of the box sides and could be tested facing up or down by flipping the box (Fig. 4). A typical plasma generated by a DBD is shown in Fig. 5.

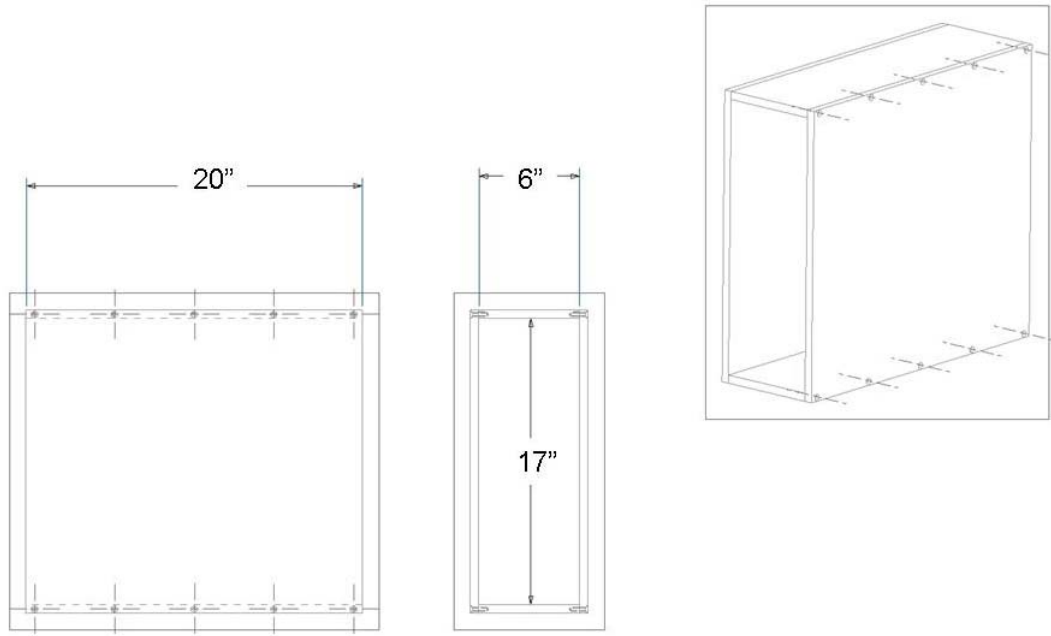


Fig. 1 Drawing of the Experimental DBD Enclosure

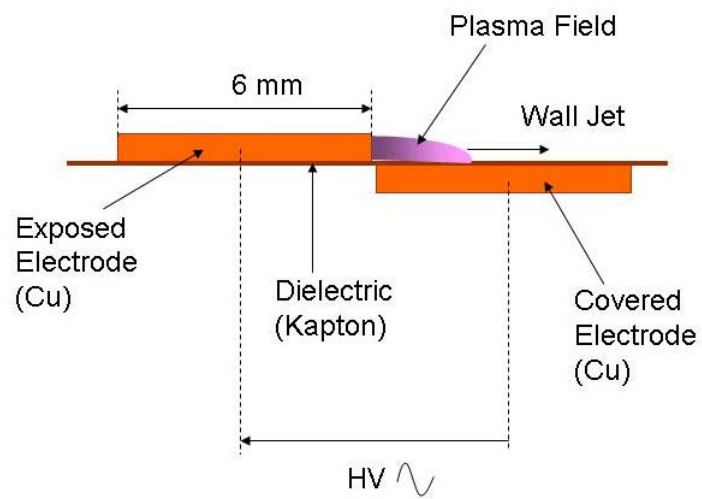


Fig. 2 DBD Side View

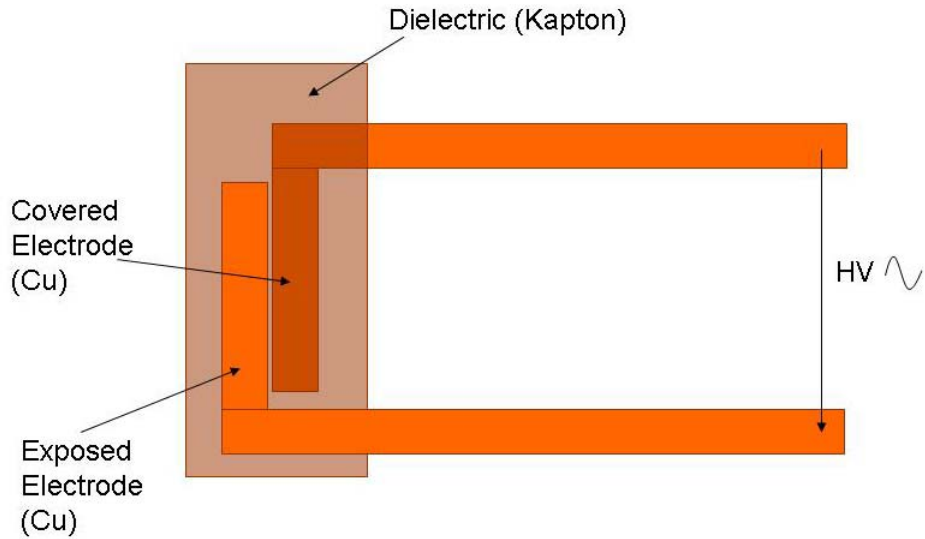


Fig. 3 DBD Top View

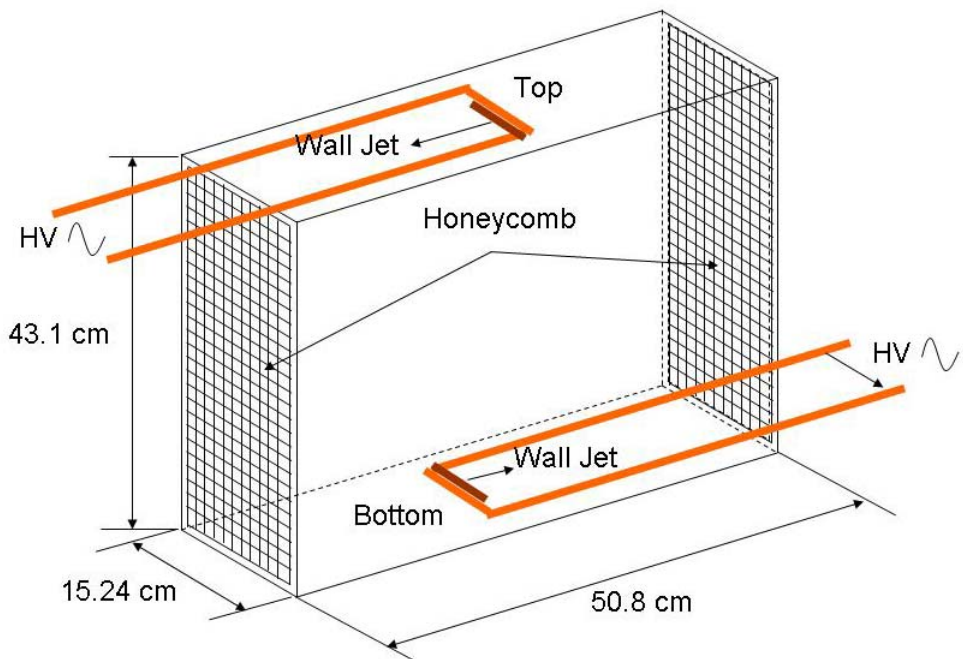


Fig. 4 DBD in the enclosure box showing the two orientations tested

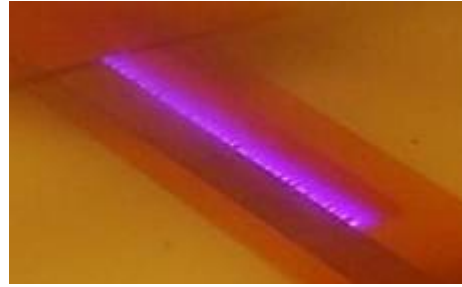


Fig. 5 Typical DBD glow

2.2 PIV

The PIV system consisted of two Nd:YAG lasers of 10 nsec pulses with maximum repetition rate of 15 Hz, a PIV camera PCO1600 (1600 x 1200 pix) with 105 mm lens and spacers for close-up views, a delay generator (Stanford DG535), and a smoke generator (Model G300) for seeding (sub-micron glycerin particles). Views with various magnifications and orientations were used to capture several relevant flow features. Views near the plasma region (Fig. 6) were used for analysis of phase-dependence with close-up (zoomed in) views. The spanwise structure of the plasma and the flow was captured with spanwise views and laser sheets near the wall (Fig. 7).

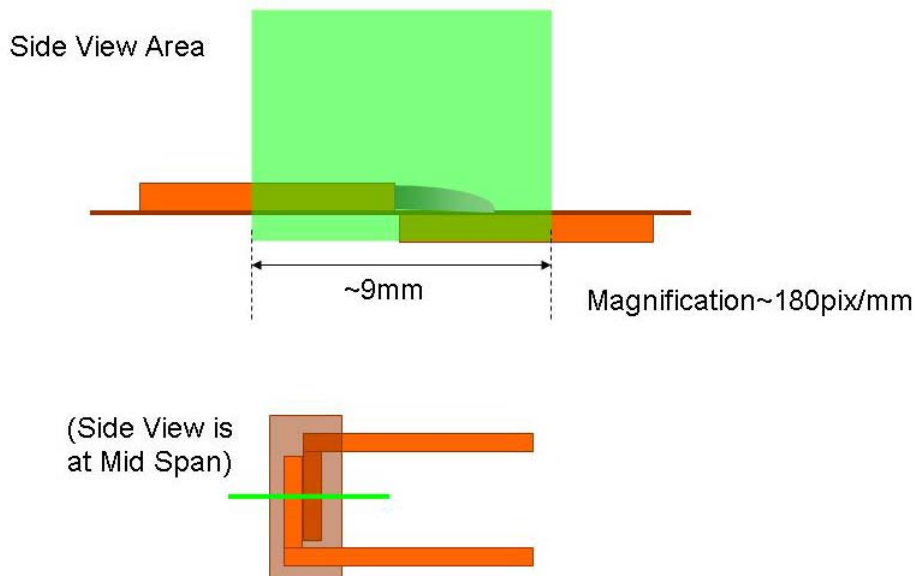


Fig. 6 PIV Side View Laser Plane and Area

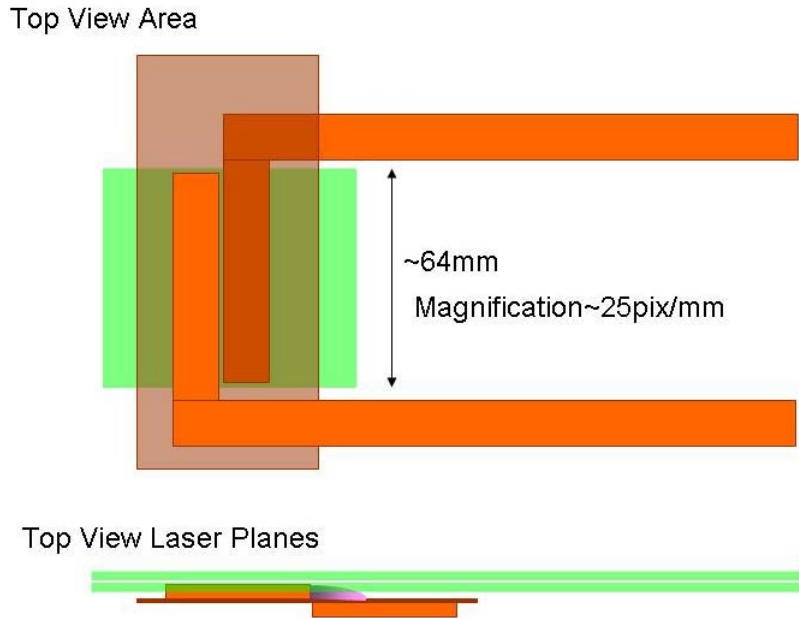


Fig. 7 PIV Top View Laser Planes and Area

2.3 Test Conditions

The high voltage waveforms were produced by a high voltage amplifier (Trek 5/80) which amplified $\times 1000$ the waves generated from wave generators (e.g. Agilent 3322A). Three waveforms (square, sinusoidal and triangular), at various amplitudes (10 kV, 5 kV, 2 kV) and frequencies (5, 2, 1.5, 1 kHz) were tested. Higher amplitudes and frequencies led to stronger plasmas and the square waveform was the strongest. Its acoustic sound level was also much louder. The phase study comprised synchronization of the waveforms, camera and lasers and data were taken at four phases of the waveforms (0, 90, 180, 270 deg.) as shown in Fig. 8. The figure shows a sample with a sinusoidal waveform, its synchronization-trigger square wave, the first PIV laser synchronized at the raising edge of the wave, and the four phases. The delay of the second laser was selected to fall within the first quarter of the wave after the first laser; some PIV experiments with longer and shorter delays were performed to corroborate that was not a major factor. The DG535 was triggered externally by the wave generator and it was used to drive the lasers and camera at 15 Hz and set the phase value. It was located far from the DBD facility to minimize electrical interferences.

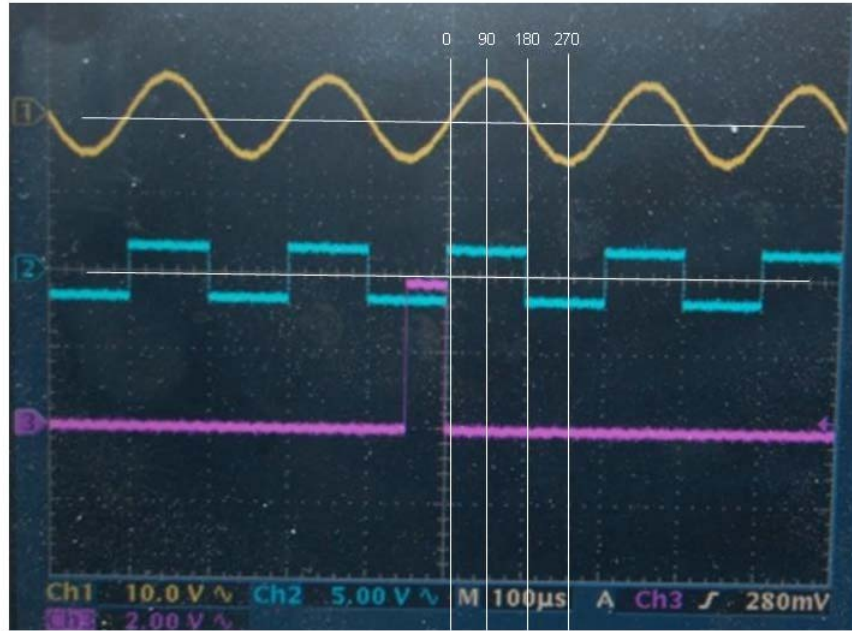


Fig. 8 Waveform samples, phases definition, and synchronization

3. Results

3.1 Reference Images

The plasma glow side-view is shown in Fig 9 for three waveforms with an exposure time of 33 msec. It is obvious that the square wave has longer range. The top (spanwise) view of the plasma shown in Fig. 10 also shows the difference in strength (given qualitatively by the range and the luminance) between the square and the sinusoidal waves. It is also obvious the filamental structure of the plasma emanating from the gap of the DBD and its coalescence into a more uniform glow. A reference picture of the electrodes at the end of a set of experiments is also shown in Fig. 10 with clear burning in the gap and over half of the buried electrode.

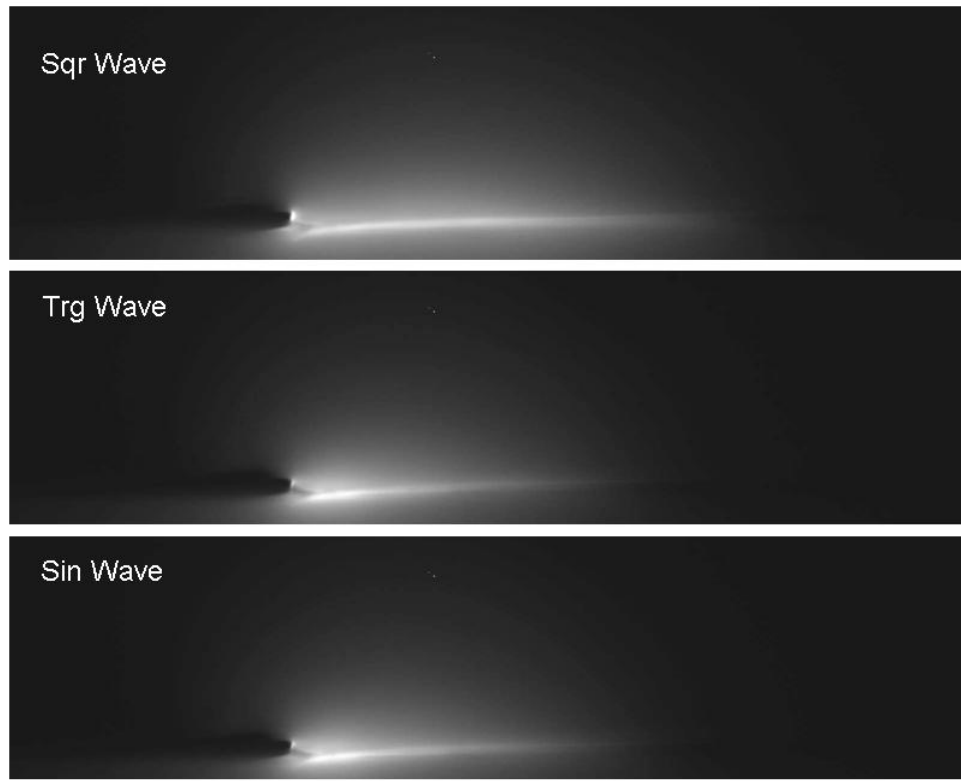


Fig.9 Sample Plasma Images (side view; 33 msec exposure)

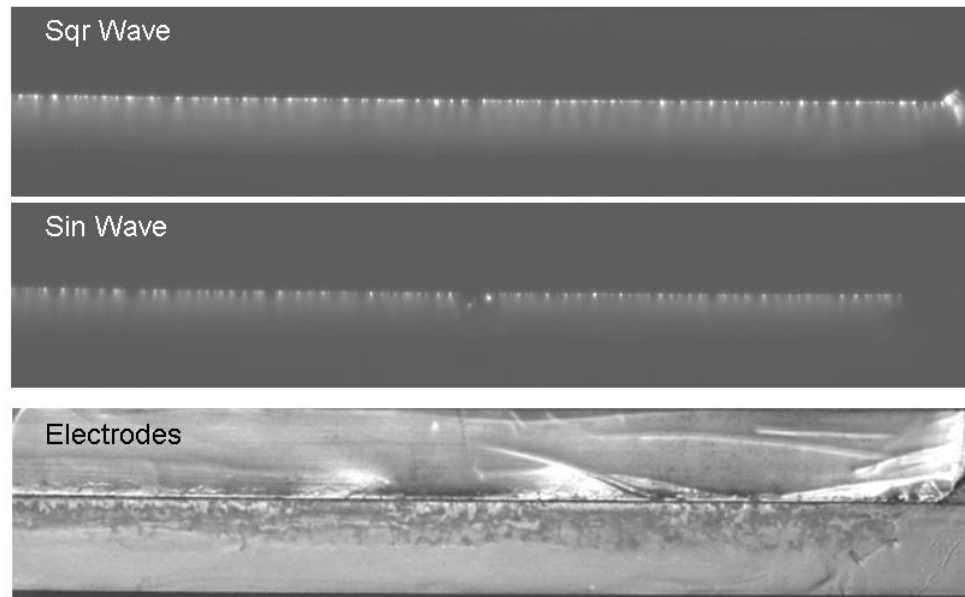


Fig.10 Sample Plasma Images (top view; 33 msec exposure) showing filamental structures and a pict of the electrodes after a set of experiments.

3.2 Flow Visualization

Typical flow visualization in a DBD is shown in Fig. 11. It includes a wall jet, a recirculation upstream of the DBD gap and an entrainment pattern of the surrounding air .

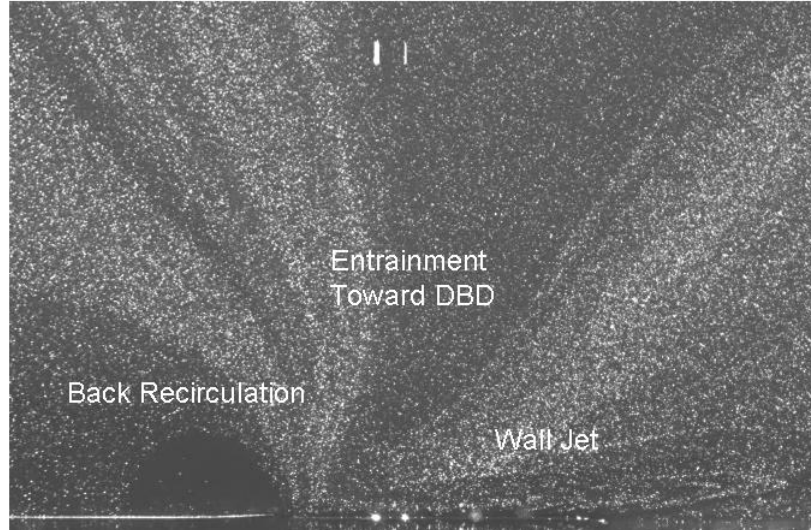


Fig. 11 Side View flow visualization of the main flow features typical of the DBD

The flow features are shown again for four phases in Figs. 12 and 13 for two frequencies of the square waveform with the DBD located in the top wall. Differences can be detected in the wall jet separation region, the extent of the recirculation area and the entrainment pattern; the lower frequency waveform having stronger differences. Comparison with other instantaneous pictures were similar for a given phase but PIV will establish these differences quantitatively. The top (spanwise) view shown in Figs. 14 and 15 clearly reveal the undulatory spanwise structure of the wall jet from its origin and its streaky structure downstream. Comparison of two instants is given in two colors in Fig. 15 to stress the repeatability of the spanwise structures. Correlation between the filamental structure of the plasma, the electrode local non-uniformities (which are enhanced by the plasma as experiment progresses) and the flow spanwise wavelength can be studied by analysis of their occurrence as shown in the superposition image of Fig. 16.

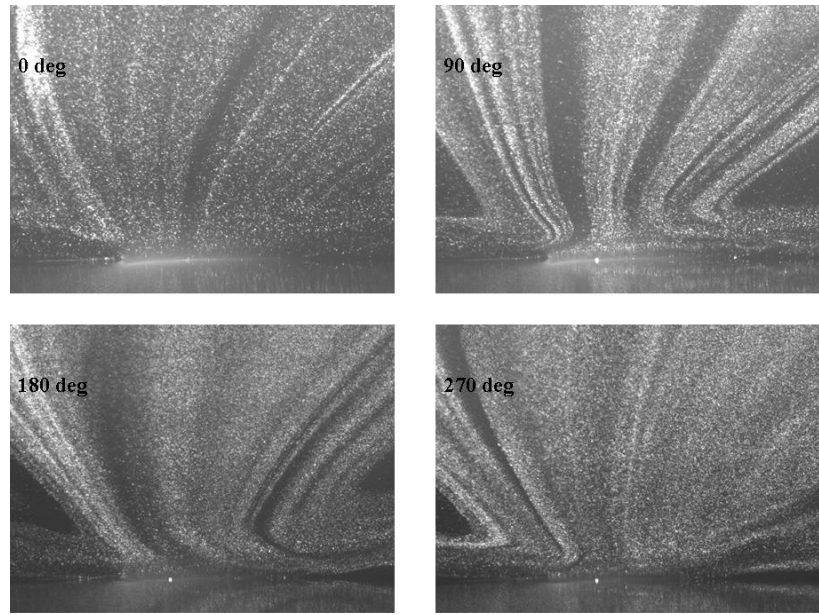


Fig. 12 Side View flow visualization of the flow features for Square Wave at 5 kHz 10 kV (four phases)

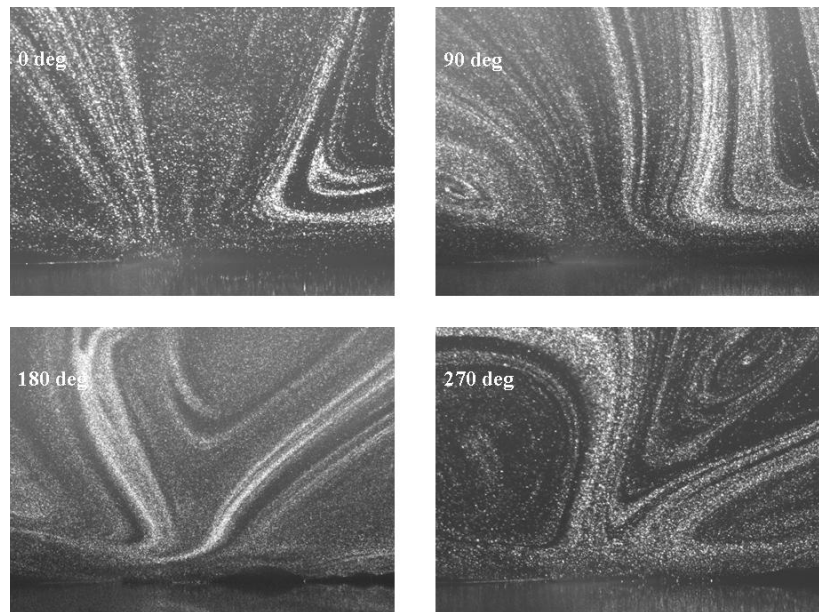


Fig. 13 Side View flow visualization of the flow features for Square Wave at 2 kHz 10 kV (four phases)

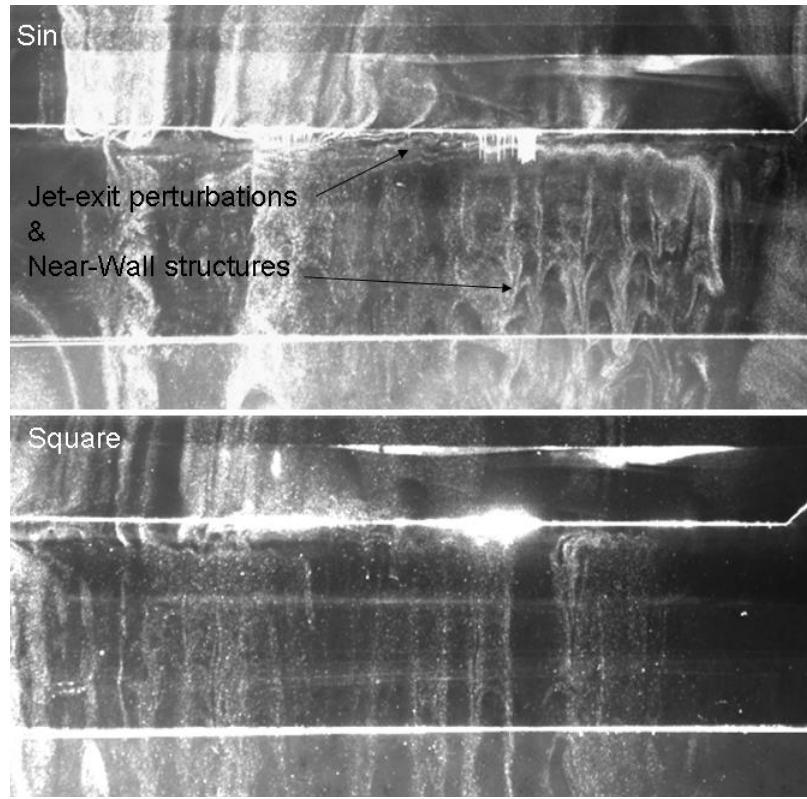


Fig. 14 Top View flow visualization of the flow features for 5 kHz, 10 kV (two waveforms)

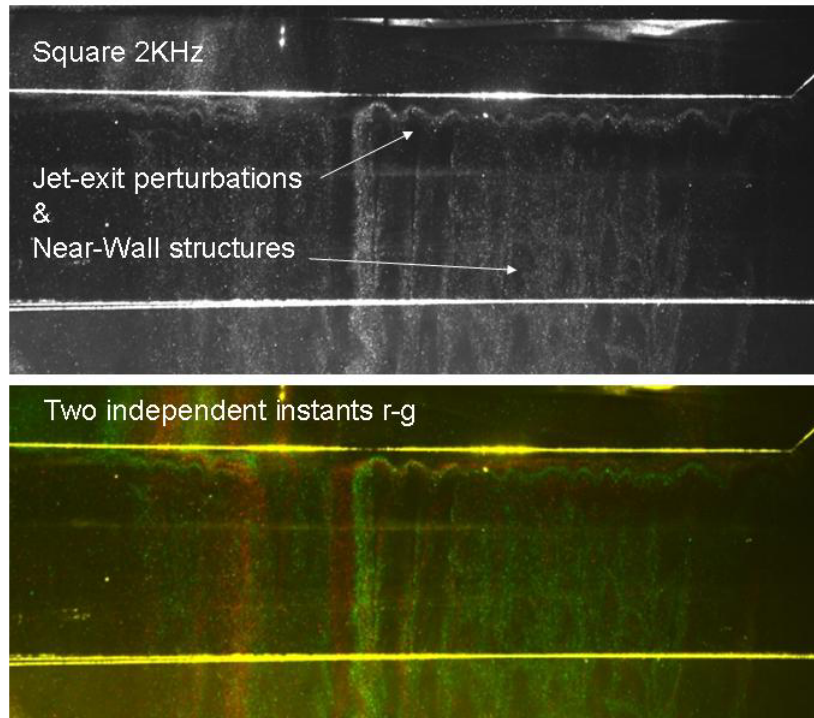


Fig. 15 Top View flow visualization of the flow features for Square Wave at 2 kHz 10 kV
(including comparison of two independent instants)

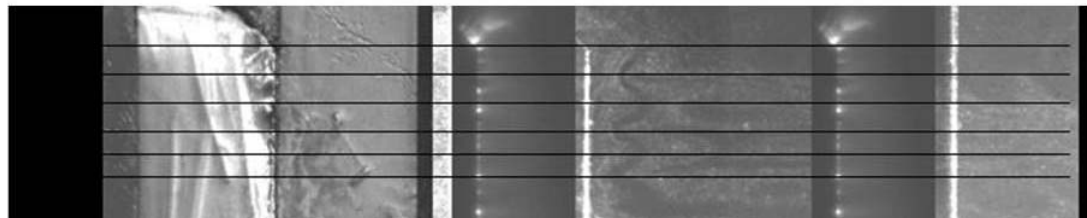


Fig. 16 Top View showing electrodes, plasma filaments, and flow streaks

3.3 PIV

The typical velocity field generated by the DBD is shown in velocity contours and vector field in Fig. 17 which corresponds to the average for the square waveform at 5 kHz at 0-phase. It shows the flow features outlined in the flow visualization section with quantitative information on the wall jet and the actual patterns surrounding the DBD, such as the recirculation area and the entrainment regions. The blank areas correspond to locations with lack of seeding. PIV was processed using ISSI software package which includes a series of algorithms typically used in PIV such as multipass iterations, filtering, etc. Seeding was kept as low as possible as to minimize the perturbation on the DBD. Heavy seeding, especially with the DBD in the bottom wall, could leave a layer of oil in the surface of the DBD and even extinguish the plasma.

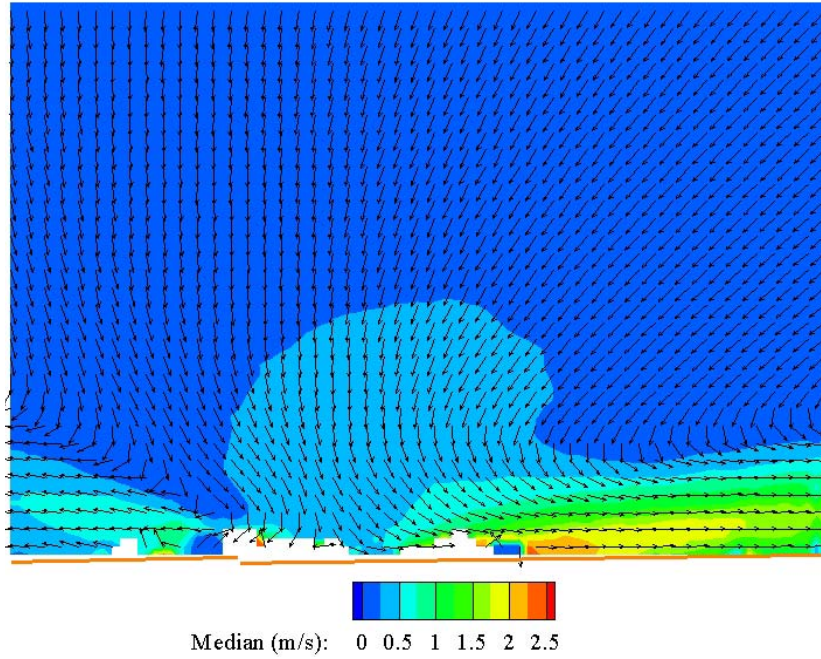


Fig. 16 Average velocity field for DBD driven with square waveform (10 kV, 5 kHz)

Various views and conditions were tested to establish a parametric characterization of the DBD flow. The velocity field for various conditions for the close-up view (Fig. 6) are most revealing --especially for the phase dependence-- and are shown next; the plots are of velocity contours with streamlines for clarity and easier comparisons between the various conditions. The average velocity field for four phases of the DBD (at top wall) driven with square waveform (10 kV, 5 kHz) is shown in Fig. 17. Clear phase differences in the wall jet, entrainment pattern, stagnation line, etc. are evident. Phase dependence is obvious with a square waveform (10 kV, 2 kHz) as shown in Fig. 18 where

a nearly a symmetry inversion of the flow patterns occurs between the raising edge and falling edge of the driving wave cycles. The variations between individual instantaneous velocity fields (e.g. Fig. 19) was minimal and concentrated in the recirculating area which takes a juncture flow pattern with unsteady secondary recirculations. These variations and those in the surrounding air could be due to large ambient air influences. The differences are similar also for the weaker waveforms (sinusoidal and triangular) shown in Figs. 20 and 21 although the phase differences are not as dramatic. With the DBD at the bottom of the wall it can be susceptible of opposite buoyancy (and possibly seeding) effects and the phase dependence is shown in Fig. 22. Finally a sample instantaneous velocity field is shown for a detail of the spanwise view (Fig. 23) with clear signature of the spanwise structure of the flow.

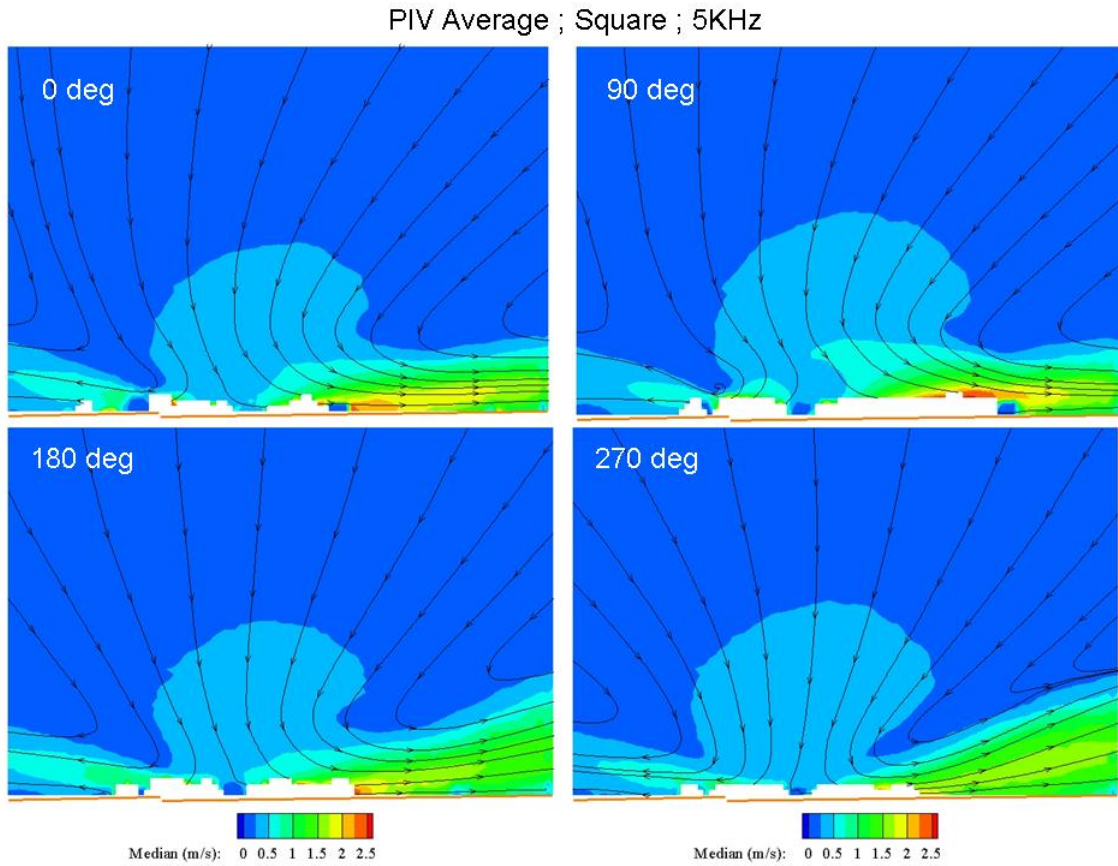


Fig. 17 Average velocity field for four phases of the DBD driven with square waveform (10 kV, 5 kHz)

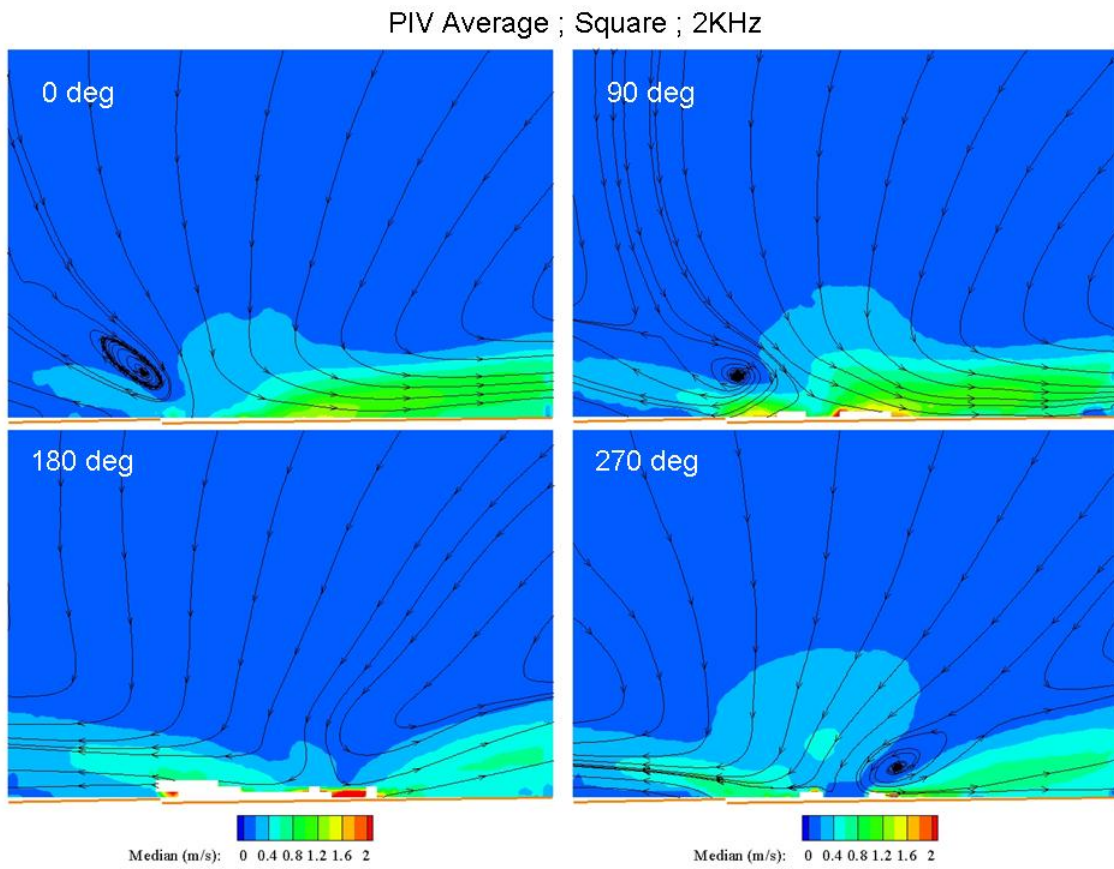


Fig. 18 Average velocity field for four phases of the DBD driven with square waveform
(10 kV, 2 kHz)

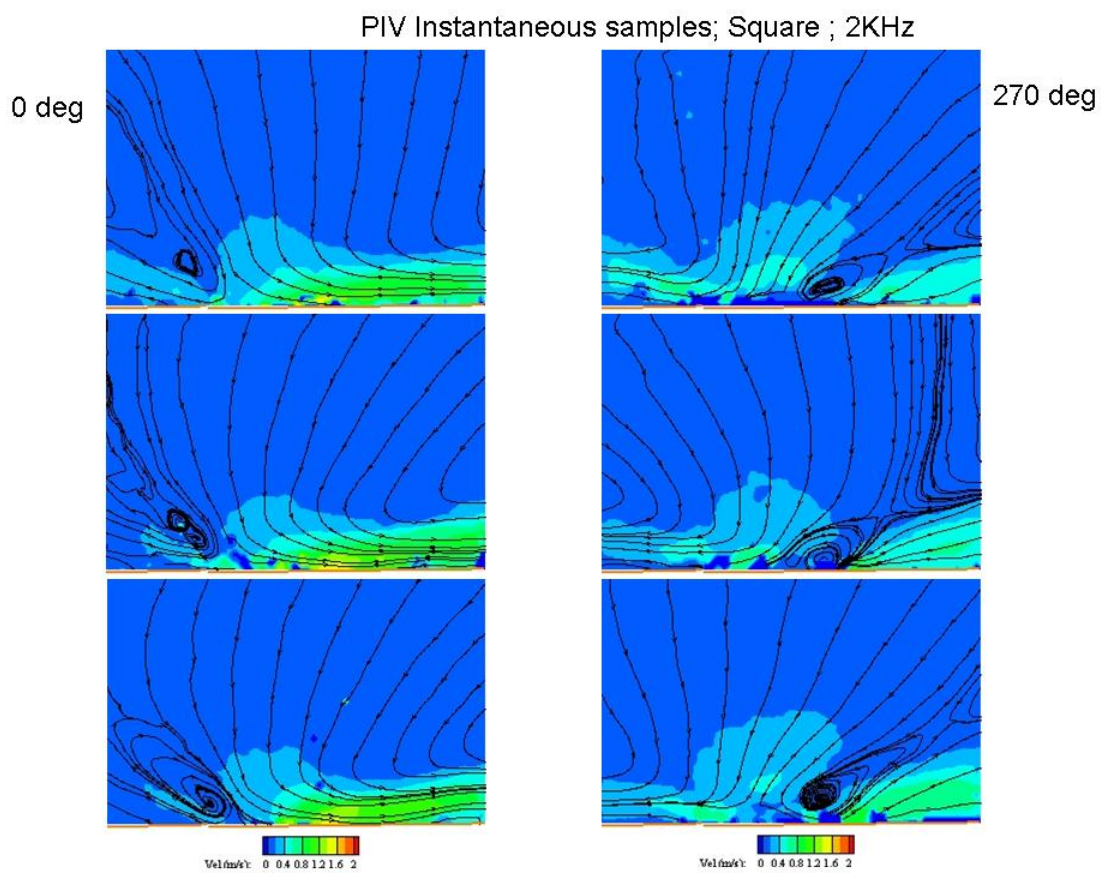


Fig. 19 Instantaneous velocity field samples for two phases of the DBD driven with square waveform (10 kV, 2 kHz)

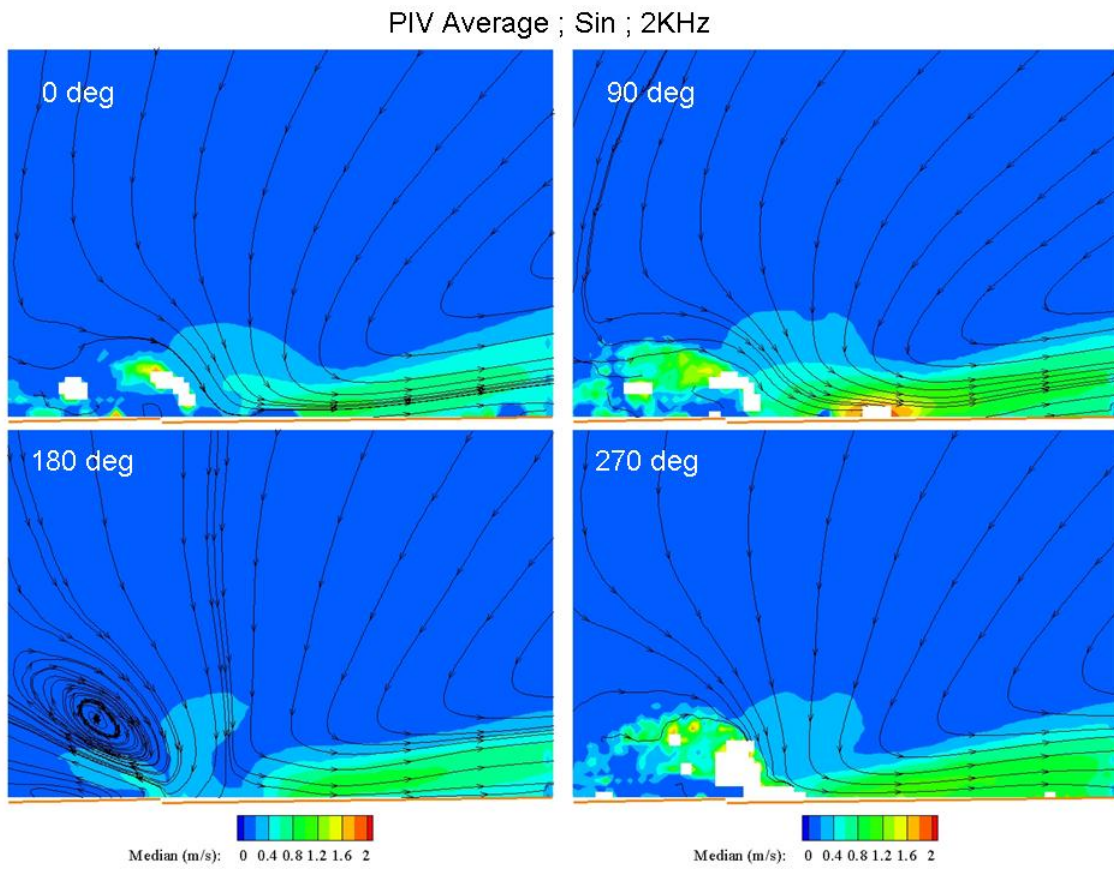


Fig. 20 Average velocity field for four phases of the DBD driven with sinusoidal waveform (10 kV, 2 kHz)

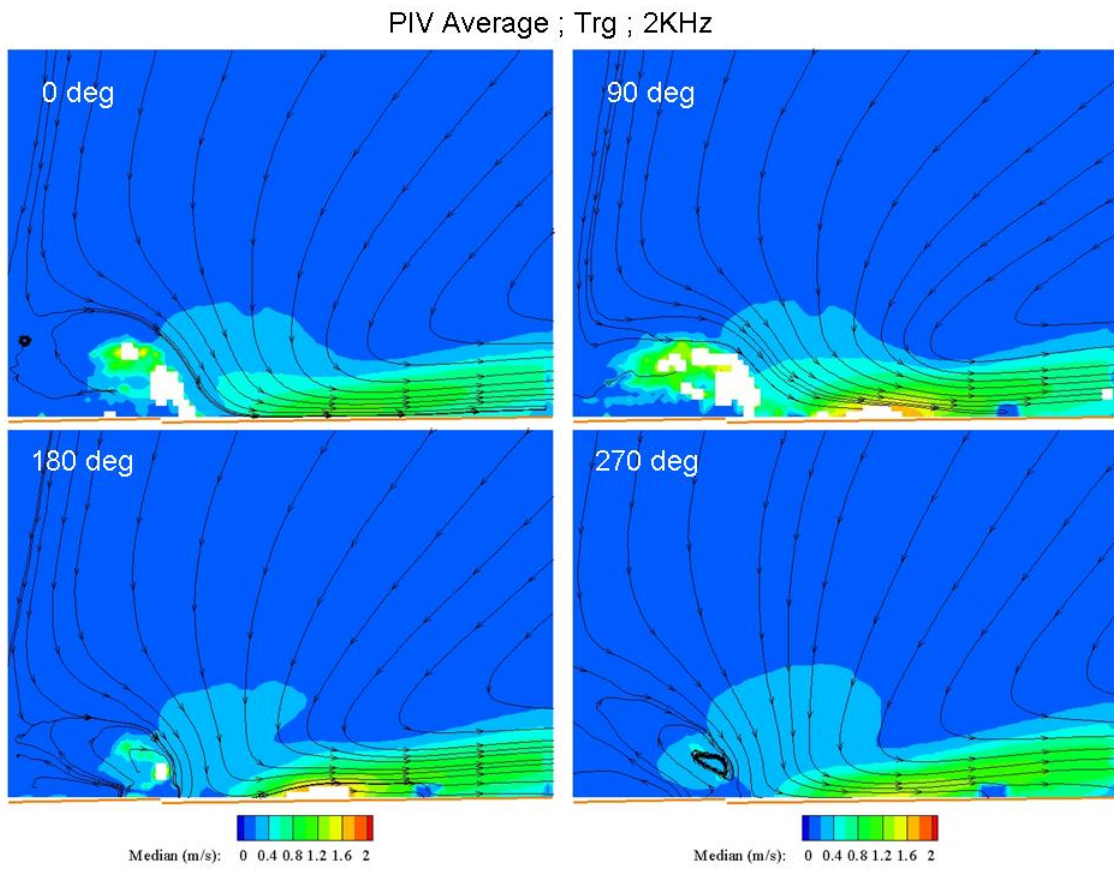


Fig. 21 Average velocity field for four phases of the DBD driven with triangular waveform (10 kV, 2 kHz)

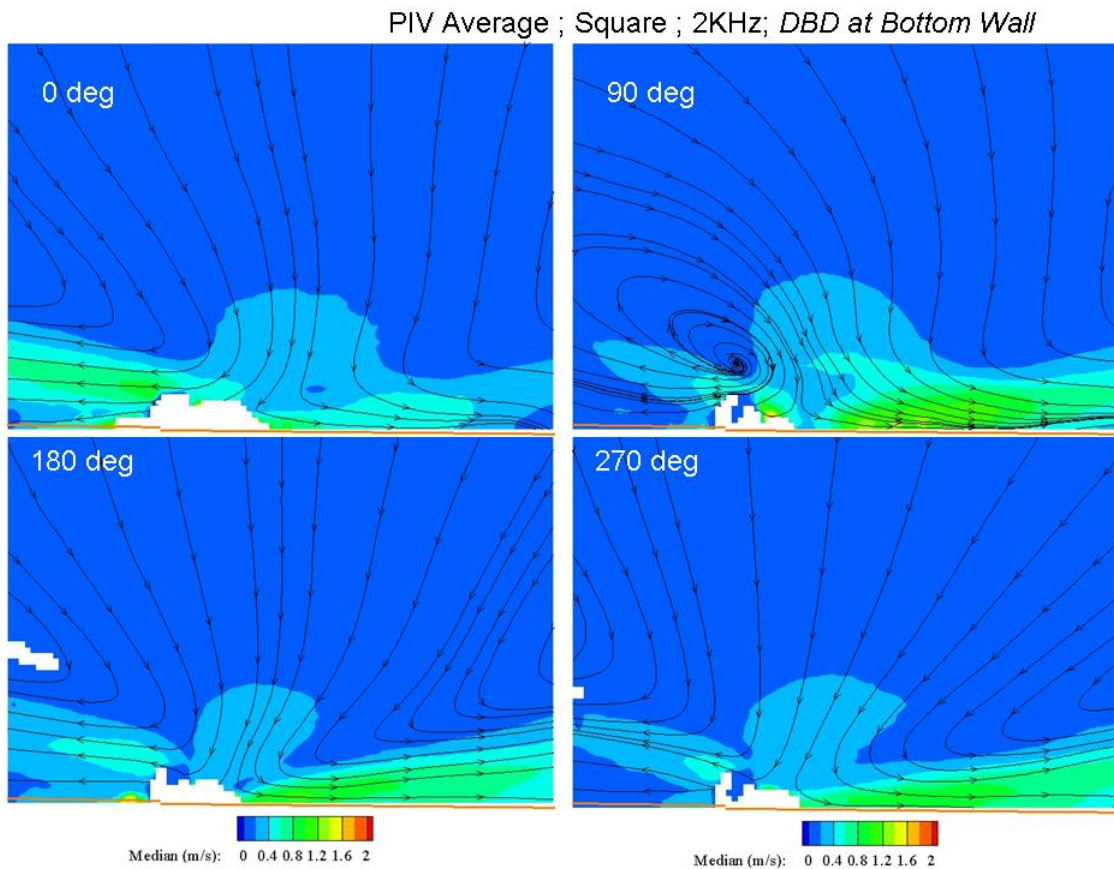


Fig. 22 Average velocity field for four phases of the DBD at the bottom wall driven with square waveform (10 kV, 2 kHz)

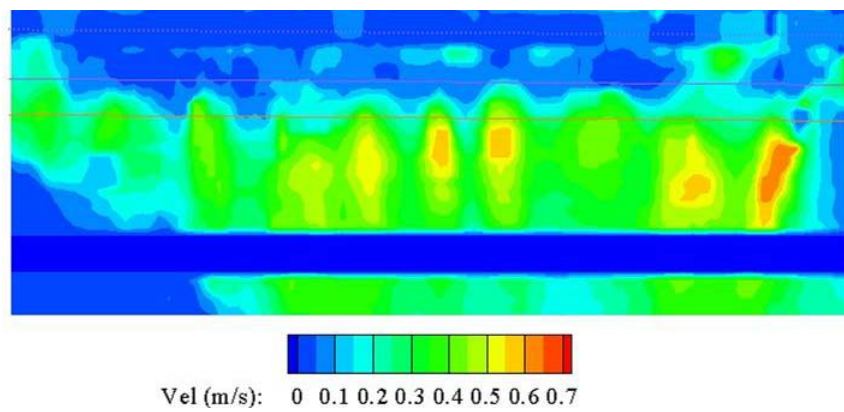


Fig. 23 Instantaneous sample of spanwise (top view) velocity field for DBD at the bottom wall driven with square waveform (10 kV, 2 kHz)